Adsorption 4, 93–111 (1998)

Mathematical Modeling of Multicomponent Nonisothermal Adsorption in Sorbent Particles Under Pressure Swing Conditions

ATANAS SERBEZOV AND STRATIS V. SOTIRCHOS
Department of Chemical Engineering, University of Rochester, Rochester, NY 14627
svs2@che.rochester.edu

Abstract. A detailed model for nonisothermal sorption of multicomponent mixtures in a single sorbent particle (monodisperse or bidisperse with negligible intracrystalline mass transport limitations) under pressure swing conditions is developed in this study. The dusty-gas model is used to describe the coupling of the molar fluxes, the temperature, the partial pressures and the partial pressure gradients of the components in the pore space of the particle. The variations of the temperature are described by an energy equation in which both convective and conductive modes of heat transport are accounted for. No limitations are imposed on the number of the components in the mixture and on the type of the adsorption isotherm. The model is applied in the investigation of the industrially important air-zeolite 5A system. Two cases with respect to the surrounding gas phase are examined: infinite environment, which is representative for single particle experiments, and finite environment, which is representative for the situation in packed bed adsorbers. It is found that in an infinite environment the external and internal temperature gradients are equally important while in a finite environment the external heat transport limitations are negligible. It is concluded that in modeling the nonisothermal operation of adsorption processes occurring in packed beds it is not necessary to allow for the temperature differences between the gas phase and the surface of the adsorbing particles. Furthermore, if the temperature gradients within the particles can be neglected, only a single temperature equation is needed to describe the energy transport in the bed.

Keywords: heat effects, pressure swing adsorption, temperature swing adsorption, multicomponent mass transport, dusty-gas model, boundary conditions

Introduction

Pressure swing adsorption (PSA) has become an important industrial operation for separation of multicomponent gaseous mixtures. In order to improve the PSA processes and develop new, more efficient PSA cycles, a detailed understanding of the behavior of the sorbent particles under pressure swing conditions is required. In a previous publication (Serbezov and Sotirchos, 1997a) we carried out a comprehensive theoretical study of the problem of multicomponent adsorption-desorption in the sorbent particles under pressure swing conditions. We examined the effects of the type of multicomponent mass transport model, the mode and the duration of pressure pulsing, the sorbent pore structure, and the type of multicomponent mixture, but in order to facilitate the analysis of the obtained computational results in terms of the aforementioned effects, we confined our study to the case of isothermal operation only. However, nonisothermal effects are intrinsic to every sorption system because of the exothermic nature of adsorption and the endothermic nature of desorption. Therefore, for a complete analysis of the problem of multicomponent adsorption and desorption in sorbent particles under pressure swing conditions, it is necessary that the multicomponent transport effects are examined in conjunction with the existing temperature gradients in the particles.

The amount of heat that is released in the particle during adsorption or absorbed during desorption varies widely from one process to another since it is determined by the heat of adsorption and the difference of

the equilibrium loadings of the adsorbing species in the multicomponent mixture between the two limits of pressure pulsing. If sorption occurs at a relatively high rate, the time provided to the released or absorbed heat to be transported to or from the surrounding gas phase may not be sufficient, and therefore, significant temperature gradients may appear in the interior of the particle. Some experimental studies (Hu and Do, 1995) have indicated that the occurrence of temperature gradients in the particles can be neglected, but there has been considerable amount of experimental evidence (Kondis and Dranoff, 1971; Lee and Ruthven, 1979; Ruthven et al., 1980; Ilavsky et al.; Haul and Stremming, 1984) that points out to the conclusion that the particles cannot be considered isothermal.

In a few mathematical models allowance has been made for the existence of temperature gradients in the interior of the adsorbing particles during the sorption process, but most of these models (Chihara et al., 1976; Brunovska et al., 1978; Sun and Meunier, 1987) consider mass transport of a single species described by an equation of the type of Fick's law, and conduction is the only mechanism of heat transport. Detailed multicomponent models for simultaneous mass and heat transport in the interior of porous media have been presented in the literature in the context of combustion (Sotirchos and Amundson, 1984a, 1984b), reaction in permeable catalysts (Lopes et al., 1995), and chemical vapor infiltration (Ofori and Sotirchos, 1996). Since the problem of transport and reaction in porous media shows many common features with the problem of transport and adsorption-desorption in adsorbing particles, these models can be employed as a basis for the formulation of nonisothermal multicomponent adsorption models.

The occurrence of bulk diffusion, Knudsen diffusion, Knudsen flow, and viscous flow during transport of gasses in porous materials is accounted in the dusty-gas model (DGM) (Jackson, 1977; Mason and Malinauskas, 1983; Sotirchos, 1989). We have used the dusty-gas model to develop a detailed multicomponent model for the simultaneous mass transport and adsorption (desorption) in sorbent particles under pressure swing conditions (Serbezov and Sotirchos, 1997a). In the present study we render that model applicable to cases where significant temperature gradients are encountered in the interior of the sorbent particle by using the general multicomponent form of the energy balance equation to describe the temperature field in the particle. The occurrence of both conductive and convective heat transport is taken into account, and allowance is made for the dependence of the transport parameters on mixture composition, temperature, and pressure. Two types of boundary conditions with respect to temperature are examined: a case where the particles are surrounded by an infinite amount of gas which results in a constant temperature of the bulk fluid, and a case where the particles are surrounded by a finite volume of gas (i.e., a case representative for the situation in a packed bed) and the temperature of the bulk gas changes as a result of the interaction with the particle. The combined effects of multicomponent transport and temperature gradients are examined by applying the nonisothermal model to the industrially important air-zeolite 5A system. Even though this is a binary system involving two gasses of similar transport properties, our past studies showed that its behavior exhibits strong multicomponent effects under pressure swing conditions (Serbezov and Sotirchos, 1997a). In order to examine the nonisothermal effects in systems with higher heats of adsorption, computations are carried out in which the heats of adsorption of the air-zeolite 5A system are increased up to an order of magnitude.

Mathematical Model

Mass and Energy Balance Equations

We consider a spherical particle of an isotropic porous adsorbent immersed in a multicomponent gaseous mixture of constant composition which is subjected to a cyclic change of the total pressure. It is assumed that the adsorbed and the fluid species within the pores are at local equilibrium (i.e., there are only macropore mass transport limitations in the system) and that the operating conditions ensure the validity of the ideal-gas law.

The mass balance equation for each species in the multicomponent mixture is written as

$$\frac{\varepsilon_p}{R_g}\frac{\partial}{\partial t}\left(\frac{p_i}{T}\right) + \nabla \cdot \underline{N}_i + (1-\varepsilon_p)\frac{\partial q_i}{\partial t} = 0 \qquad (1)$$

ε_p is the porosity of the adsorbing particle, p_i is the partial pressure of species i in the bulk of the particle, T is the temperature, R_g is the ideal gas law constant, $\underline{N}_i$ is the molar flux of species i within the particle

relative to stationary coordinates, and q_i is the equilibrium loading of species i defined per unit volume of solid.

When the particles cannot be considered isothermal, an energy balance equation must be added to the system of mass balance equations. Starting from the local enthalpy balance in the particle and using Eq. (1), the energy equation can be written in the general form as

$$\left[\frac{1}{R_g T}\sum_{i=1}^{n}\varepsilon_p C_{pg,i}\,p_i + \sum_{i=1}^{n}(1-\varepsilon_p)C_{pq,i}q_i + (1-\varepsilon_p)\rho_s C_{ps}\right]\frac{\partial T}{\partial t} + \sum_{i=1}^{n}(-\Delta H_i)\frac{\partial q_i}{\partial t} + \sum_{i=1}^{n}\underline{N}_i\cdot(C_{pg,i}\nabla T) - \nabla\cdot\lambda^e\nabla T = 0 \qquad (2)$$

$C_{pg,i}$ is the specific heat capacity of species i in the gas phase, $C_{pq,i}$ is the specific heat capacity of species i in the adsorbed phase, C_{ps} is the specific heat capacity of the solid material, ρ_s is the density of the solid phase, $(-\Delta H_i)$ is the heat of adsorption of species i, and λ^e is the effective thermal conductivity of the sorbent particle. The contributions of the gas phase and the adsorbed phase heat capacities, i.e., the terms $\frac{1}{R_g T}\sum_{i=1}^{n}\varepsilon_p C_{pg,i}\,p_i$ and $\sum_{i=1}^{n}(1-\varepsilon_p)C_{pg,i}q_i$ may be much smaller than the term $(1-\varepsilon_p)\rho_s C_{ps}$ and in such a case, they can be neglected without a significant effect on the results.

Boundary Conditions.

At $r = 0$

$$N_i = 0 \qquad (3)$$

$$\nabla T = 0 \qquad (4)$$

At $r = R_p$

$$p_i = P_{b,T}\,y_{b,i};\ y_{b,i} = \text{ const} \qquad (5)$$

$$-\lambda^e\nabla T\cdot\mathbf{n} = h_f\left(T_{R=R_p} - T_b\right) \qquad (6)$$

R_p is the radius of the particle and $y_{b,i}$, $P_{b,T}$, and T_b are the mole fraction of species i, the total pressure, and the temperature, respectively, of the gas phase surrounding the particle, h_f is a heat transfer coefficient, and $\mathbf{n}$ is the unit vector in the surrounding gas normal to the external surface of the particles. For a particle existing in an adsorbing bed, the values of $y_{b,i}$, $P_{b,T}$, and T_b are determined by the overall mass and energy balances in the bed. Under typical conditions of operation, the total pressure changes with approximately the same rate at every point in the bed. To simplify the analysis and the discussion of the results, it will be assumed that the mole fraction of the gaseous species in the gas phase surrounding the particle, $y_{b,i}$, remain constant while the total pressure changes according to the prescribed pulsing sequence. Two different cases will be considered for the ambient temperature T_b: a case in which its value remains constant, and another, in which the surrounding gas phase is of finite volume, and its temperature is determined by the rate at which it exchanges heat with the particle. The second case is more relevant to the actual situation of pellets existing in a packed bed and interacting with little volume of gas phase. The equation used to determine the variation of T_b with time will be presented and discussed later in conjunction with the computational results.

Initial Condition. The initial condition for each half-cycle is the final condition of the previous one. At the onset of the process the bulk phase inside the particle has uniform composition and temperature, the same as the surrounding gas mixture.

Adsorption Isotherms. When the adsorption isotherm is an explicit function of the partial pressures and the temperature, i.e.,

$$q_i = q_i(p_1, p_2, \ldots, p_n, T) \qquad (7)$$

the quantity $\frac{\partial q_i}{\partial t}$ that appear in Eqs. (1) and (2) can be expressed in terms of the time derivatives of the partial pressures and the temperature using the chain rule of differentiation:

$$\frac{\partial q_i}{\partial t} = \sum_{j=1}^{n}\frac{\partial q_i}{\partial p_j}\frac{\partial p_j}{\partial t} + \frac{\partial q_i}{\partial T}\frac{\partial T}{\partial t} \qquad (8)$$

In the case of linear adsorption isotherm, i.e.,

$$q_i = \frac{h_i(T)}{R_g T}p_i = \frac{a_i\exp(d_i/T)}{R_g T}p_i \qquad (9)$$

we have

$$\frac{\partial q_i}{\partial t} = \frac{a_i\exp(d_i/T)}{R_g T^3}\left[T^2\frac{\partial p_i}{\partial t} - (d_i + T)\,p_i\frac{\partial T}{\partial t}\right] \qquad (10)$$

Intraparticle Mass Transport Equations

The purpose of the intraparticle mass transport model is to replace the terms $\nabla \cdot \underline{N}_i$ and $\underline{N}_i$ in Eqs. (1) and (2) by more specific mathematical expressions. A comprehensive discussion of the intraparticle mass transport models applicable to sorbent particles under pressure swing conditions has been previously provided by Serbezov and Sotirchos (1997a). For multicomponent systems the dusty-gas model (Jackson, 1977; Mason and Malinauskas, 1983; Sotirchos, 1989) has been recognized as the most rigorous among the existing mass transport models. It accounts for bulk diffusion, Knudsen diffusion, Knudsen flow, and viscous flow in the particle. It is written as

$$\left(\nabla p_i + \frac{B^e P_T}{\mu}\frac{y_i}{D^e_{K,i}}\nabla P_T\right) = -R_g T\left(\sum_{j\neq i}\frac{y_j\underline{N}_i - y_i\underline{N}_j}{\mathscr{D}^e_{i,j}} + \frac{\underline{N}_i}{D^e_{k,i}}\right). \quad (11)$$

$\mathscr{D}^e_{i,j}$ and $D^e_{K,i}$ are the effective binary diffusion coefficient of the $[i, j]$ pair and the Knudsen diffusion coefficient of species i, respectively. They are related to temperature, pressure, and the structure of the porous medium by the equations:

$$\mathscr{D}^e_{i,j} = \hat{\mathscr{D}}_{i,j}\left(\frac{\hat{P}_T}{P_T}\right)\left(\frac{T}{\hat{T}}\right)^{3/2} S_1 \quad (12)$$

$$D^e_{K,i} = \hat{D}_{K,i}\left(\frac{T}{\hat{T}}\right)^{1/2} S_2 \quad (13)$$

$\hat{\mathscr{D}}_{i,j}$ and $\hat{D}_{K,i}$ are reference quantities computed at reference total pressure $\hat{P}_T$, reference temperature $\hat{T}$, and reference pore radius $\hat{r}_p$. S_1, S_2, and B^e are structural characteristics of the porous medium. Their values can be determined by experimentation or by theoretical methods once a physical model for the pore structure of the system is adopted. The formulae for the calculation of the transport parameters are listed in Table 1.

For the DGM, an analytical expression for $\underline{N}_i$ and $\nabla \cdot \underline{N}_i$ is not possible because the model is implicit in the fluxes. However, it is possible to compute these values numerically at every spatial and temporal position by casting the DGM in vector-matrix form:

$$\mathbf{F}\nabla\mathbf{p} = \mathbf{B}\underline{\mathbf{N}} \quad (14)$$

Table 1. Formulae used for the calculation of the mass transport properties.

Effective transport coefficients		
Coefficient	Equation	Reference
$\mathscr{D}^e_{i,j}$	$\mathscr{D}^e_{i,j} = \hat{\mathscr{D}}_{i,j}\left(\frac{\hat{P}_T}{P_T}\right)\left(\frac{T}{\hat{T}}\right)^{3/2} S_1$	
	$\hat{\mathscr{D}}_{i,j} = 2.628\times10^{-3}\frac{\sqrt{\hat{T}^3(M_i+M_j)/(2M_iM_j)}}{\hat{P}_T\sigma^2_{i,j}\omega\,\mathscr{D}_{i,j}}$	Chapman-Enskog equation Bird et al. (1960)
	$S_1 = \frac{\varepsilon_p}{\eta_B}$	
$D^e_{K,i}$	$D^e_{K,i} = \hat{D}_{K,i}\left(\frac{T}{\hat{T}}\right)^{1/2} S_2$	
	$\hat{D}_{K,i} = 97\hat{r}_p\left(\frac{\hat{T}}{M_i}\right)^{1/2}$	Present (1958)
	$S_2 = \frac{\varepsilon_p}{\eta_K}\frac{r_p}{\hat{r}_p}$	
$\frac{B^eP_T}{\mu}$	$\mu = \sum_{i=1}^{n}\frac{y_i\mu_i}{\sum_{j=1}^{n}y_j\Phi_{i,j}}$	Semiempirical formula of Wilke Bird et al. (1960)
	$\Phi_{i,j} = \frac{1}{\sqrt{8}}\left(1+\frac{M_i}{M_j}\right)^{-1/2}\left[1+\left(\frac{\mu_i}{\mu_j}\right)^{1/2}\left(\frac{M_j}{M_i}\right)^{1/4}\right]^2$	
	$B^e = \frac{\varepsilon_p r_p^2}{\eta_V 8}$	

p is the vector of the partial pressures of the species and $\underline{\mathbf{N}}$ is the vector of the molar fluxes of the species. **B** and **F** are $[n \times n]$ matrices whose elements are:

$$B_{i,i} = -R_g T \left(\sum_{j \neq i} \frac{p_j}{\mathscr{D}^e_{i,j}} + \frac{1}{D^e_{K,i}} \right) \tag{15}$$

$$B_{\substack{i,j \\ j \neq i}} = R_g T \left(\frac{p_i}{\mathscr{D}^e_{i,j}} \right) \tag{16}$$

$$F_{i,j} = \left(1 + \frac{B^e p_i}{\mu D^e_{K,i}} \right) \tag{17}$$

$$F_{\substack{i,j \\ j \neq i}} = \left(\frac{B^e p_i}{\mu D^e_{K,i}} \right) \tag{18}$$

The values of $\underline{N}_i$ are found upon inversion of Eq. (14). The values of $\nabla \cdot \underline{N}_i$ are calculated by first differentiating Eq. (14) and then solving it for $\nabla \cdot \underline{\mathbf{N}}$. We have

$$\underline{\mathbf{N}} = \mathbf{B}^{-1} \mathbf{F} \nabla \mathbf{p} \tag{19}$$

$$\nabla \cdot \underline{\mathbf{N}} = \mathbf{B}^{-1} (\nabla \mathbf{F} \cdot \nabla \mathbf{p} + \mathbf{F} \nabla^2 \mathbf{p} - \nabla \mathbf{B} \cdot \underline{\mathbf{N}}) \tag{20}$$

$\nabla \mathbf{B}$ and $\nabla \mathbf{F}$ are matrices whose elements are $\nabla B_{i,j}$ and $\nabla F_{i,j}$, respectively.

Computational Method

The mathematical model is solved numerically using a collocation scheme based on B-spline interpolation (De Boor, 1978). The spatial domain is divided into N intervals by means of $(N+1)$ break points. In each interval the spatial variables (i.e., partial pressures and temperature) are approximated by a fourth order (cubic) polynomial. The separate polynomial pieces are joined at the breakpoints by requiring continuity of each function and its first spatial derivative. The mass and energy balance equations are discretized in space by requiring that they be satisfied at two collocation points for each interval and the boundary conditions be valid at the end points. The discretization procedure reduces each equation in the model (we have n mass balance and one energy equations) from a partial differential equation to a system of $2N$ ordinary differential equations with respect to time and 2 algebraic equations which come from the boundary conditions. For a mixture of n components and N intervals the mathematical model is transformed to a system of $2(n+1)N$ ordinary differential equations and $2(n+1)$ algebraic equations. The integration of the resulting sets of algebraic and ordinary differential equations is carried out by a Gear-type solver (Gear, 1971). Additional information on the numerical scheme is given by Sotirchos (1991).

If the DGM equations are not incorporated in the mass and energy balance equations, they can be discretized by the foregoing procedure producing $n(2N+2)$ algebraic equations. Consequently, the total size of the system that has to be solved by the differential-algebraic solver almost doubles.

Results and Discussion

In order to investigate the nonisothermal effects in sorbent particles under pressure swing conditions, we apply the developed nonisothermal multicomponent model to the industrially important system O_2-N_2-zeolite 5A. The parameters used in the computations are listed in Table 2. In our computations we have neglected the terms $\frac{1}{R_g T} \sum_{i=1}^{n} \varepsilon_p C_{pg,i} p_i$ and $\sum_{i=1}^{n} (1-\varepsilon_p) C_{pg,i} q_i$ in Eq. (2) based on the assumption that they are much smaller than the term $(1-\varepsilon_p)\rho_s C_{ps}$. The temperature dependence of the heat capacities, the heats of sorption, and the effective thermal conductivity, as well as the composition dependence of the viscosity, are neglected, and the values of these parameters at the ambient conditions (i.e., $P_T = 0.1$ MPa, $T = 300$ K, $y_{O_2} = 0.21$, $y_{N_2} = 0.79$) are used in the computations. However, the numerical code was constructed for the general case of nonisothermal operation, and therefore, it can readily be applied to include all the terms in Eq. (2) and the temperature dependence of all the parameters that appear in it.

The zeolite 5A sorbent particles considered here have a bidispersed structure in the sense that the zeolite crystals are bound together in a macroporous matrix. Haq and Ruthven (1986) and Ruthven and Xu (1993) have studied the sorption and diffusion of O_2 and N_2 in zeolite 5A commercial pellets and have concluded that intracrystalline diffusion is fast enough to be neglected as a mass transport resistance. Surface diffusion can also be neglected as a mass transport mechanism because of the small amount of adsorbed species on the pore space of the large pore network of the zeolites, i.e., the external surface of the microparticles (Alpay et al., 1993). Therefore, all the important mass transport mechanisms in the zeolite 5A particles are accounted for in the developed model, that is, bulk diffusion, Knudsen diffusion, Knudsen flow, and viscous flow.

Table 2. Parameters used in the computations.

Surface gas phase composition	
y_{N_2}	79 mol%
y_{O_2}	21 mol%
Adsorbent	
Type	Zeolite 5A
Porosity, ε_p	0.4
Density of the solid carcass, ρ_s	2×10^3 kg/m^3
Specific heat capacity of the solid carcass, C_{ps}	10^3 J/kg·K
Effective thermal conductivity, λ^e	0.5 J/m·s·K
Adsorption coefficients, $h_i(T) = a_i \exp(d_i/T)$	
a_{N_2}	4.55×10^{-3}[a], 2.46×10^{-3}[b]
a_{O_2}	0.0363[a], 0.015[b]
d_{N_2}	2.405×10^3[a], 2.645×10^3[b] K
d_{O_2}	1.450×10^3[a], 1.740×10^3[b] K
Heat of sorption	
ΔH_{N_2}	22.76×10^6[a] J/kmol
ΔH_{O_2}	14.77×10^6[a] J/kmol
Heat capacity of the gaseous species	
C_{pg,N_2}	26.4×10^3 J/kmol·K
C_{pg,O_2}	29.2×10^3 J/kmol·K
Thermal conductivity of the gas mixture, k_g	0.038 J/m·s·K
Temperature, T	300 K
Lower operating pressure, $P_{t,\text{low}}$	0.1 MPa

[a]Data from Haq and Ruthven (1986).
[b]Data from Sorial et al. (1983).

Adsorption isotherms for O_2 and N_2, on zeolite 5A have been reported in several studies (Sorial et al., 1983; Haq and Ruthven, 1986; Miller et al., 1987). All experimental data show that it is reasonable to accept that up to approximately 0.3 MPa the adsorption isotherms of O_2 and N_2 on zeolite 5A are linear and independent, that is, the adsorption of each component depends only on its own partial pressure. The temperature dependence of the adsorption coefficients is given by Eq. (9). Figure 1 presents the adsorption coefficients of O_2 and N_2 as function of temperature in the range 280–320 K for the data of Sorial et al. (1983) and Haq and Ruthven (1986). The two sets of data are similar in the temperature range shown in Fig. 1. In our computations we have used the values reported by Haq and Ruthven (1986).

It is seen from Fig. 1 that a ratio of approximately 1 : 3 exists between the adsorption coefficients of O_2 and N_2 at all temperatures in the temperature range shown in the figure, indicating that even though the adsorption capacity of the sorbent varies with the temperature, the separation factor remains almost constant. Since the temperature dependence of the adsorption coefficients is moderate, the effects on the behavior of the process that result from the temperature dependence of the adsorption isotherms are not expected to be dramatic even for significant temperature gradients.

The ranges over which the various parameters that appear in the energy equation (Eq. (2)) vary in typical adsorption applications are listed in Table 3. Comparing the heats of adsorption for O_2 and N_2 and the thermal properties of zeolite 5A with the ranges of values in Table 3, we conclude that the O_2-N_2-zeolite 5A system must be representative of an intermediate situation with regard to the magnitude of the intraparticle temperature gradients.

The formulae used for the calculation of the transport coefficients are summarized in Table 1. In order to determine the structural parameters of the porous medium, the latter is approximated by an array of long cylindrical capillaries randomly oriented in the three-dimensional space. The value of 3 is used for the tortuosity factors.

Table 3. Typical values of the parameters in the energy equation for adsorption systems.

Adsorbent	
Density of the solid carcass, ρ_s	$(1.5–2.5) \times 10^3$ kg/m^3
Specific heat capacity of the solid carcass, C_{ps}	$(0.8–1.0) \times 10^3$ J/kg·K
Effective thermal conductivity, λ^e	(0.4–0.8) J/m·s·K
Heat of adsorption, ΔH_i	$(10–50) \times 10^6$ J/kmol
Heat capacity of the gaseous species, $C_{pg,i}$	$(30–40) \times 10^3$ J/kmol·K

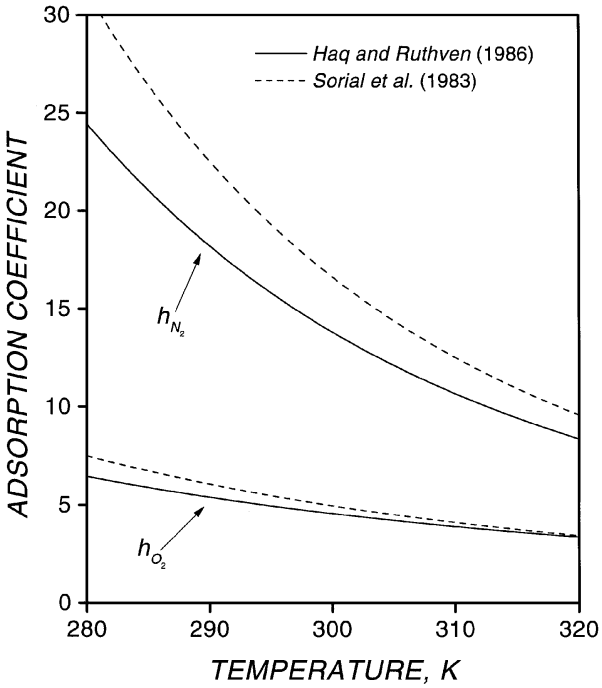

Figure 1. Adsorption coefficients for O_2 and N_2 on zeolite 5A vs. temperature.

We have employed three different patterns of total pressure cycling, in all of which we have alternated between pressurization and depressurization with equal times.

1. Stepwise pressurization and stepwise depressurization.
   Pressurization:
   $$P_T = P_{T,\text{high}}, \quad 0 \le t \le t_{1/2} \tag{21}$$
   Depressurization:
   $$P_T = P_{T,\text{low}}, \quad 0 \le t \le t_{1/2} \tag{22}$$
   where $t_{1/2}$ denotes the duration of the half-cycle.
2. Linear pressurization and exponential depressurization.
   Pressurization:
   $$P_T = P_{T,\text{low}} + \frac{P_{T,\text{high}} - P_{T,\text{low}}}{t_{1/2}} t, \quad 0 \le t \le t_{1/2} \tag{23}$$
   Depressurization:
   $$P_T = P_{T,\text{low}} + (P_{T,\text{high}} - P_{T,\text{low}}) e^{-\gamma t}, \quad 0 \le t \le t_{1/2} \tag{24}$$
3. Sinusoidal total pressure change.
   $$P_T = P_{T,\text{low}} + \frac{P_{T,\text{high}} - P_{T,\text{low}}}{2} + \frac{P_{T,\text{high}} - P_{T,\text{low}}}{2} \times \sin\left[\frac{2\pi}{t_{\text{cycle}}}\left(t - \frac{t_{\text{cycle}}}{4}\right)\right] \tag{25}$$

The stepwise pressurization and depressurization are often used to test and validate intraparticle mass transport models but in real PSA processes the adsorbing particles are seldom exposed to such conditions. At many instances in PSA operations, the pressurization is carried out at constant molar flow rate. It can be shown that if the mass transport limitations are negligible, the total pressure in the adsorbing bed increases linearly with time (Serbezov and Sotirchos, 1994). For depressurization, experimental results show that the total pressure in the column decreases exponentially (Farooq et al., 1993). Therefore, the cycle with linear pressurization and exponential depressurization is a more realistic test case than stepwise pressurization and stepwise depressurization. In some PSA processes, such as rapid PSA, the pressurization and the depressurization are carried out by connecting the adsorbing bed to surge tanks kept at constant pressure. However, the step changes in the total pressure at the ends of the column are smeared out because of the mass transport limitations in the adsorbing bed. Therefore, a sinusoidal change in the total pressure at the outer surface of the adsorbing particles is more representative of the conditions inside the adsorbing bed.

Results for Particles in an Infinite Environment with no External Heat Transport Limitations

We first consider the case in which the particle exists in an infinite environment, and as a result, the heat absorbed or released in it cannot affect the ambient temperature, which is assumed to remain at a fixed value. In order to be able to investigate the change of temperature in the interior of the particles separately from the temperature change that may occur because of the presence of heat transfer limitations from the bulk of the gas phase to the particle surface, we first present and discuss results obtained without external heat transfer limitations, that is, for fixed temperature at the external surface of the particles.

Dynamic Response of the Particles. Figures 2, 3, and 4 present dynamic responses of the sorbent particle to different modes of pressure change at the surface. The variation of the dimensionless loading at the center of the particles during the first three cycles is shown in Fig. 2 for O_2 and in Fig. 3 for N_2. The total loading at ambient composition, total pressure and temperature is used throughout this study to render the loadings of the components in dimensionless form. The variation of the temperature at the center of the particle during the first three cycles is shown in Fig. 4. The duration of the half cycle time is 3 s which is chosen so that at the end of each half cycle the particle is equilibrated with the surrounding environment. Comparison of Figs. 2 and 4 shows that at the center of the particle the temperature variation follows qualitatively the variation of the dimensionless loading of O_2. In the case of instantaneous pressurization, the temperature at the center of the particle rises rapidly and decreases at a slower rate, approaching the ambient (surface) temperature. This behavior is consistent with the experimental observations of Ilavsky et al. (1980). The highest temperature change, about 6 K during pressurization and 7 K during depressurization, is observed in the case of instantaneous pressure change in the beginning of each half cycle. For the other modes of pressure change the temperature variation is less than 3 K, but since the pressure is varied smoothly, the particle is never thermally equilibrated with the surrounding environment.

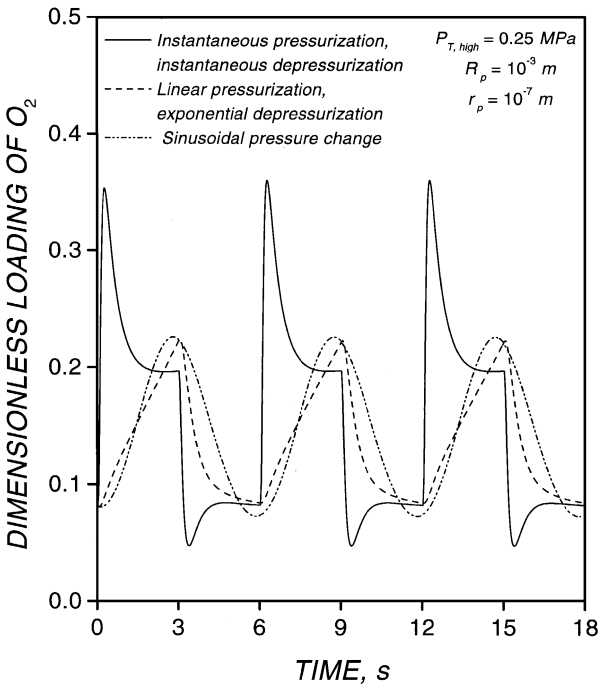

Figure 2. Dimensionless loading of O_2 in a binary mixture of O_2 and N_2 at the center of a sorbent particle as function of time for the first three cycles with instantaneous pressurization/depressurization, linear pressurization/exponential depressurization ($\gamma = 1\ s^{-1}$), and sinusoidal pressure change.

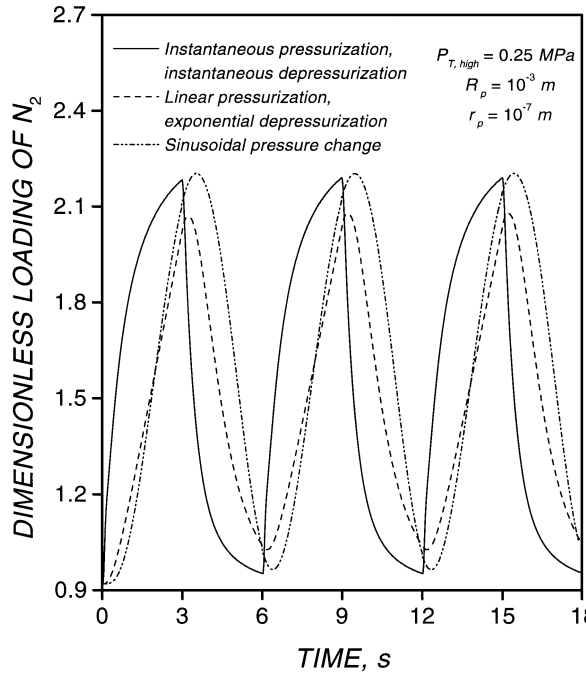

Figure 3. Dimensionless loading of N_2 in a binary mixture of O_2 and N_2 at the center of a sorbent particle as function of time for the first three cycles with instantaneous pressurization/depressurization, linear pressurization/exponential depressurization ($\gamma = 1\ s^{-1}$), and sinusoidal pressure change.

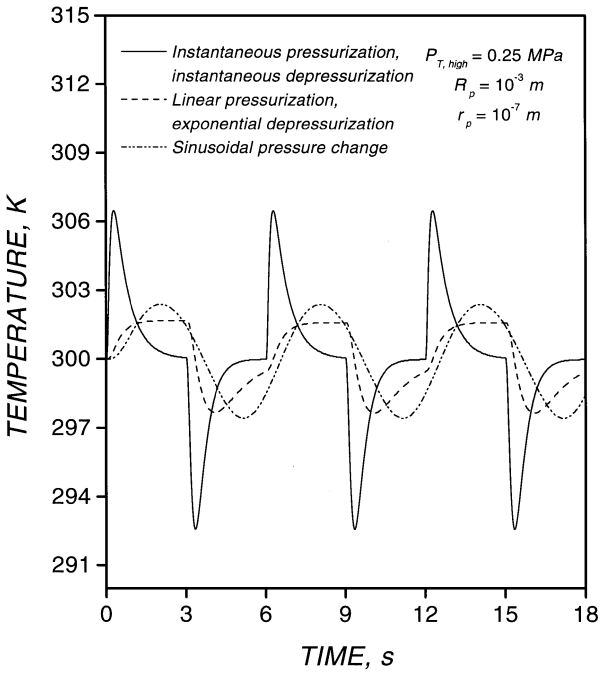

Figure 4. Temperature at the center of a sorbent particle as function of time for the first three cycles with instantaneous pressurization/depressurization, linear pressurization/exponential depressurization ($\gamma = 1\ s^{-1}$), and sinusoidal pressure change.

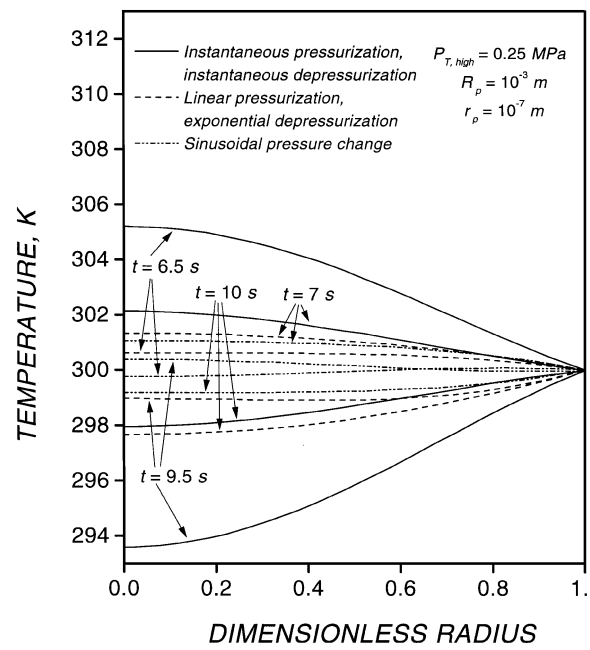

Figure 5. Temperature in a sorbent particle as function of the dimensionless radius at four time instances during the second cycle of instantaneous pressurization/depressurization, linear pressurization/exponential depressurization ($\gamma = 1\ s^{-1}$), and sinusoidal pressure change (Fig. 4).

Since O_2 is the less adsorbable species in the mixture, it is transported faster in the interior of the adsorbing particle. In the case of instantaneous pressure change O_2 is the main contributor to the total pressure equilibration within the particle, but once the total pressure is equilibrated, O_2 starts diffusing backwards. As a result, in Fig. 2 we observe an initial increase in the dimensionless loading of O_2 at the center of the particle which is followed by a decrease to the equilibrium loading. In the case of N_2 (Fig. 3) the dimensionless loading at the center of the particle during instantaneous total pressure change increases or decreases monotonically. These effects are discussed in detail by Serbezov and Sotirchos (1997b).

Figure 5 shows the temperature profiles in the particle at four time instances during the second cycle of Fig. 4 for all pressure pulsing schemes. In all cases the temperature profile increases or decreases monotonically from the surface to the center. Thus, the difference between the temperatures at the center and at the surface of the particle gives the largest temperature difference that can be experienced at any location in the particle. This difference takes its value largest for the case of instantaneous pressure change, but, as we pointed out earlier, this situation is not encountered in real PSA operations. For more realistic cases (e.g., linear pressurization/exponential depressurization and sinusoidal pressure change), the intraparticle temperature profiles in Fig. 5 suggest that for the air-zeolite 5A system the assumption of uniform temperature in the particle is not unreasonable.

Effect of the Cycle Time. Figures 6 and 7 present results of the same conditions as in Figs. 2–5 but with 0.5 s half cycle time, that is, a value smaller by a factor of 6. This value is chosen so that at the end of each half cycle the particle is not equilibrated with the surrounding environment. Figure 6 shows the temperature variation during the first three cycles at the center of the particle for three different schemes of pressure change, whereas Fig. 7 presents the variation of the dimensionless loading of O_2 during the first three cycles at the center of the particle for instantaneous pressure change for both isothermal and nonisothermal operation. We concluded from the results in Figs. 2–5 that the maximum temperature rise or drop in the particle depends on the rates of pressurization and depressurization with the largest differences encountered for

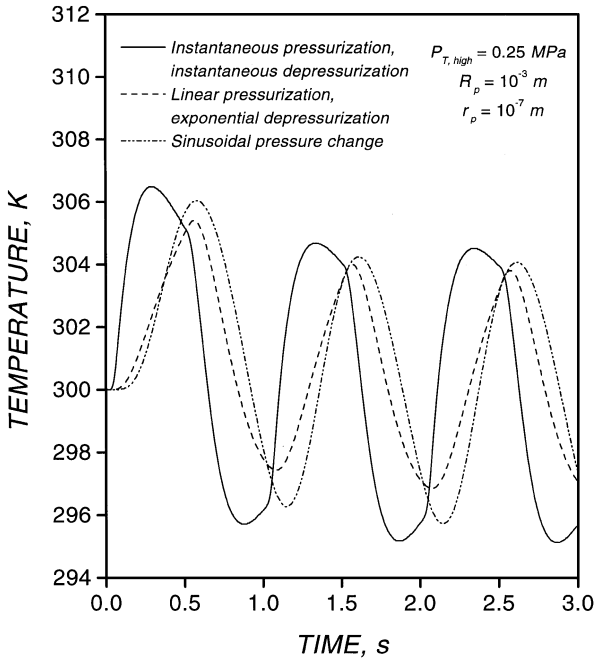

Figure 6. Temperature at the center of a sorbent particle as function of time for the first three cycles with instantaneous pressurization/depressurization, linear pressurization/exponential depressurization ($\gamma = 6\ s^{-1}$), and sinusoidal pressure change.

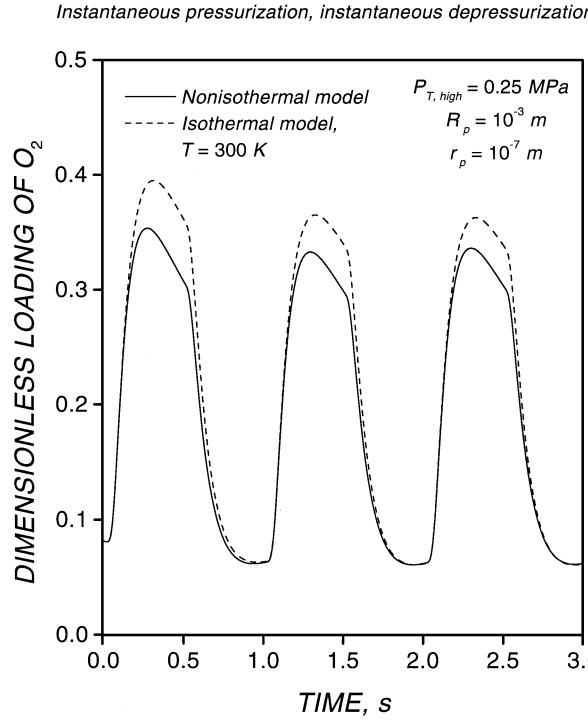

Figure 7. Dimensionless loading of O_2 in a binary mixture of O_2 and N_2 at the center of a sorbent particle as function of time for the first three cycles with instantaneous pressurization/depressurization. Comparison between isothermal and nonisothermal models for short cycle times.

instantaneous pressure change. Figure 6 shows that this conclusion is also valid for smaller cycle times. The comparison of the results of Figs. 4 and 6 indicates that as the cycle time decreases the maximum temperature difference (rise or drop) from the ambient temperature increases for the continuous pressurization schemes. This is a direct result of the higher pressurization (depressurization) rate which causes higher rates of heat generation or absorption in the interior of the particles. The rate of pressurization is independent of the cycle time for the instantaneous pressure scheme and a comparison of Figs. 4 and 6 reveals that the history of the temperature at the center of the particle in the first half cycle (pressurization) is identical for the two cycle times. However, this is not the case for the subsequent half cycles. The duration of the half cycle time in Fig. 6 is not large enough to equilibrate the particle with its environment, and thus, depressurization and pressurization after the first half cycle are initialized from a nonequilibrated state. This leads to a decrease in the maximum temperature drop or rise that is observed in the particles during those half cycles.

Figure 7 shows that the dimensionless loading of O_2 at the center of the particle has a lower value during pressurization when the existence of temperature gradients is taken into account. The opposite behavior is exhibited during depressurization. The difference between the isothermal and the nonisothermal results does not appear to be large enough to warrant inclusion of intraparticle temperature gradients in the mathematical model for adsorption in a single particle at the conditions of Fig. 7. The effects of the temperature gradients on the dimensionless loading histories of O_2 and N_2 can be explained by considering the temperature dependence of the adsorption coefficients of O_2 and N_2. Equation (9) and Fig. 1 show that an increase in the temperature leads to a decrease of the adsorption coefficients, and hence, an increase of the effective rate of transport of the two species in the pore space of the particles. However, it decreases the relative difference between the adsorption coefficients of O_2 and N_2, and thus, lowers the overshoot of O_2. The opposite situation occurs during depressurization, but since the particle starts from a nonequilibrated state after the first half cycle, it is not easy to compare the isothermal and nonisothermal particle histories for the subsequent half cycles. A better picture of the effects of

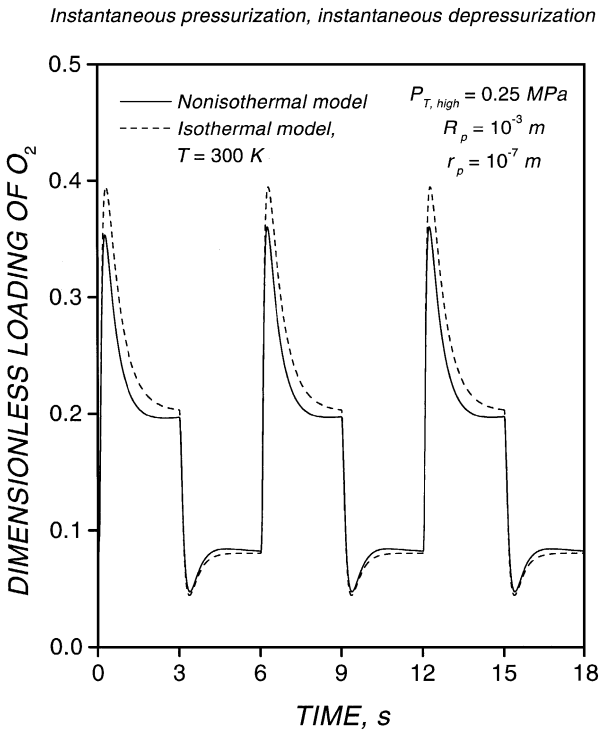

Figure 8. Dimensionless loading of O_2 in a binary mixture of O_2 and N_2 at the center of a sorbent particle as function of time for the first three cycles with instantaneous pressurization/depressurization. Comparison between isothermal and nonisothermal models for long cycle times.

the thermal gradients is offered by the results in Fig. 8 where the cycle time is the same as in Figs. 2–5, and therefore, more time is provided for equilibration.

Effect of the Pulsing Pressure Limits. The effects of the difference between the pulsing pressure limits in the nonisothermal behavior of the particles are examined in Fig. 9 which shows the temperature variation during the first three cycles at the center of the particle for three different modes of pressure change. The parameters and the conditions are the same as those used in Fig. 4 with the exception of the high limit of the operating pressure which is increased from 0.25 MPa in Fig. 4 to 0.4 MPa in Fig. 9. The same qualitative behavior is exhibited by the temperature at the center of the particle in Figs. 4 and 9 but the temperature differences in Fig. 9 are by about a factor of 2 larger than those in Fig. 4. For linear isotherms—as it is the case in Figs. 4 and 9—(the amounts of species adsorbed or desorbed, and hence, the heat released or absorbed is proportional to the difference between the pressure pulsing limits.

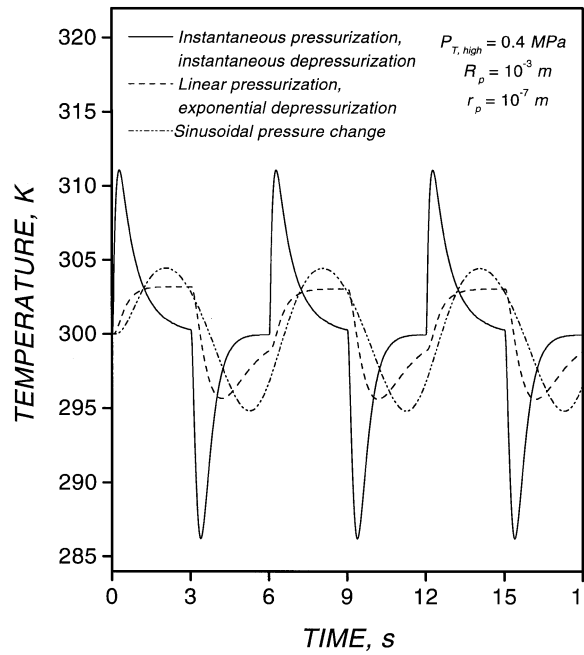

Figure 9. Temperature at the center of a sorbent particle as function of time for the first three cycles with instantaneous pressurization/depressurization, linear pressurization/exponential depressurization ($\gamma = 1\ s^{-1}$), and sinusoidal pressure change. Effect of the pulsing pressure limits.

The difference between the high and the low pressure limits in Fig. 9 ($P_{T,\text{high}} - P_{T,\text{low}} = 0.3$ MPa) is twice that in Fig. 4 ($P_{T,\text{high}} - P_{T,\text{low}} = 0.15$ MPa), and this is why the temperature differences in Fig. 9 are about two times larger than those in Fig. 4.

Effects of Pore Size and Particle Size. To examine effects of pore size, we present in Figs. 10 and 11 the response of the temperature and the dimensionless loading of O_2 at the center of the particle at the same conditions as those used in Figs. 2–4, but for pore size equal to 10^{-8} m. Figure 10 gives the history of the temperature at the center of the particle during the first three cycles for the all three different modes of pressure change, whereas Fig. 11 presents results only for the case of instantaneous pressure change during isothermal and nonisothermal operation.

Comparison of the results in Figs. 4 and 2 with those shown in Figs. 10 and 11, respectively, reveals that decreasing the pore size slows down the considerably the response of the pellet and leads to smaller temperature differences in its interior. This behavior is a direct consequence of the fact that Knudsen diffusivity and the viscous permeability are proportional to the pore

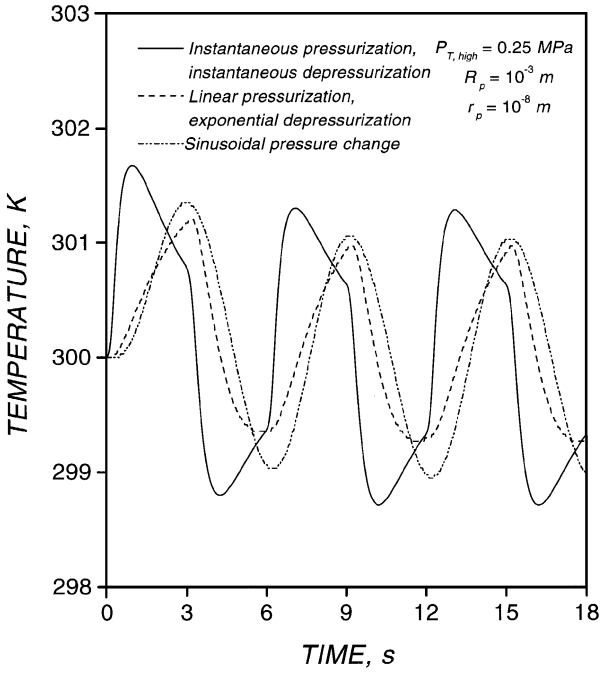

Figure 10. Temperature at the center of a sorbent particle as function of time for the first three cycles with instantaneous pressurization/depressurization, linear pressurization/exponential depressurization ($\gamma = 1\ s^{-1}$), and sinusoidal pressure change. Effect of the particle pore size.

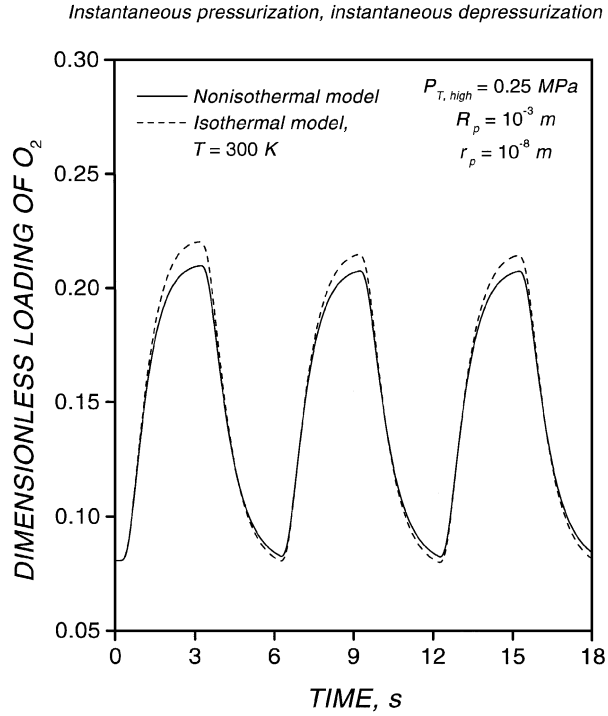

Figure 11. Dimensionless loading of O_2 in a binary mixture of O_2 and N_2 at the center of a sorbent particle as function of time for the first three cycles with instantaneous pressurization/depressurization. Comparison between isothermal and nonisothermal models for small particle pore sizes.

radius and its square, respectively, (Table 1), and therefore, the decrease in the pore size increases the resistance for mass transport in the interior of the particles. The decreased rates of adsorption and desorption lead to lower rates of heat release and consumption, respectively, in the particle. This in turn causes smaller temperature differences in the interior of the particle because the decrease of the pore size does not affect the rate at which heat is transported by conduction in the pellets.

By casting the mass and energy balance equations of the mathematical model in dimensionless form, one readily concludes that the only parameter or variable in which the particle size appears is the dimensionless time $\tau = t\frac{\mathscr{D}^e}{R_p^2}$. This suggests that if the particle size is changed, the responses of the particles expressed in dimensionless time units will remain the same, provided that the rate of pulsing is scaled accordingly. An increase of the particle size increases the effective resistance for mass transport and heat transport in the particle, but since both are increased by the same factor (i.e., R_p^2), their ratio remains the same.

Results for Particles in an Infinite Environment with External Heat Transport Limitations

To examine the effect of the presence of external heat transport limitations on the behavior of the response of the temperature and the loading, computations were carried out at the conditions of Figs. 2–5 for finite values of h_f, or equivalently, the Nusselt number. The Nusselt number is related to the heat transfer coefficient in the stagnant layer surrounding the particle, h_f, by the expression

$$\mathrm{Nu} = \frac{2R_p h_f}{k_{g,\mathrm{mix}}} \tag{26}$$

where $k_{g,\mathrm{mix}}$ is the thermal conductivity of the gas mixture. The results of these computations are presented in Figs. 12–14.

Figure 12 shows the variation of the temperature at the external surface of the particles for different values of the Nusselt number ($\mathrm{Nu} = 2$, $\mathrm{Nu} = 10$, $\mathrm{Nu} = 100$, and $\mathrm{Nu} = 1000$). The case of $\mathrm{Nu} = 2$ is a limiting case

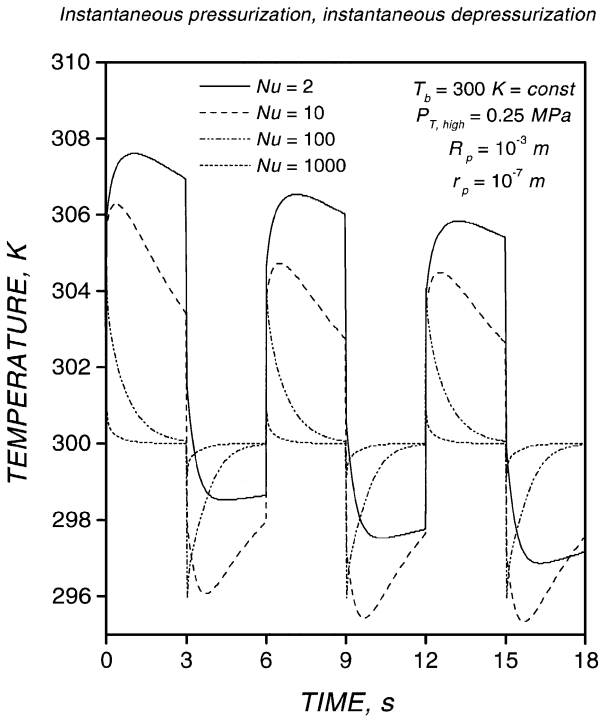

Figure 12. Temperature at the center of a sorbent particle in an infinite environment as function of time for the first three cycles with instantaneous pressurization/depressurization. Effect of the external mass transport limitations for moderate heats of adsorption.

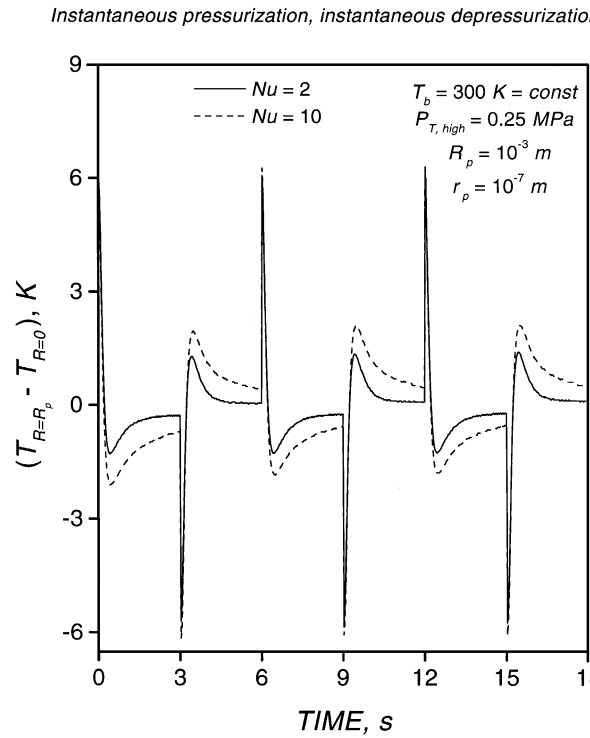

Figure 13. Temperature difference between the surface and the center of a sorbent particle in an infinite environment as function of time for the first three cycles with instantaneous pressurization/depressurization. Effect of the external mass transport limitations for moderate heats of adsorption.

which corresponds to a sphere exposed to an infinite stagnant environment. In agreement with our expectations, Fig. 12 shows that the excursions of the surface temperature from the ambient conditions decrease with the increase of the Nusselt number, and almost die out for Nu = 1000. It can also be seen that the number of cycles necessary for the particle to reach cyclic steady state decreases, as the Nusselt number increases. For Nu = 100 and Nu = 1000 the cyclic steady state is reached immediately, because at the end of each half cycle the surface temperature becomes equal to the ambient temperature which is the initial condition for the process. This is not the case for Nu = 2 and Nu = 10 where the external heat transport limitations are too large and an equality between the temperatures at the surface of the particle and in the bulk of the gas phase cannot be reached within the time limits of the half cycle (i.e., 3 s). The initial conditions for the second cycle are different from the ambient conditions (i.e., the initial conditions for the first cycle) as a result of which the maxima and minima of the temperature response at the surface of the particle move downwards until a new state of dynamic equilibrium is established between the particle and the environment in which the temperature response is symmetrical with respect to the ambient temperature (300 K).

Figures 13 and 14 present the temperature difference between the surface and the center of the particle and the dimensionless loading of O_2 at the center of the particle for two Nusselt numbers (Nu = 2 and Nu = 10). Comparison between Figs. 13 and 14 and Figs. 4 and 2, respectively, shows that the maximum internal temperature rise or drop and the dimensionless loading do not change significantly in the presence of external heat transport limitations. However, the decrease of the Nusselt number influences the time at which the temperature maxima or minima occur by shifting them towards smaller time values. For small Nusselt numbers there is also a change in the sign of the temperature difference as it approaches the ambient value.

Comparison between Figs. 12 and 13 shows that the maximum external temperature difference is

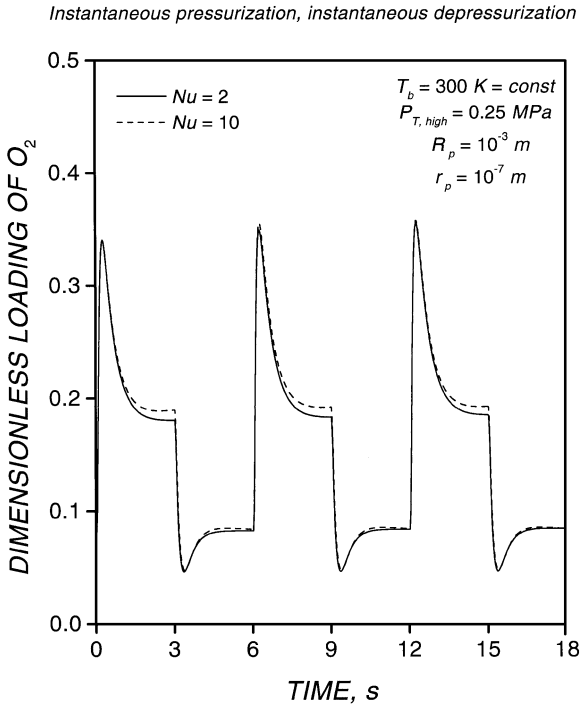

Figure 14. Dimensionless loading of O_2 in a binary mixture of O_2 and N_2 at the center of a sorbent particle in an infinite environment as function of time for the first three cycles with instantaneous pressurization/depressurization. Effect of the external mass transport limitations for moderate heats of adsorption.

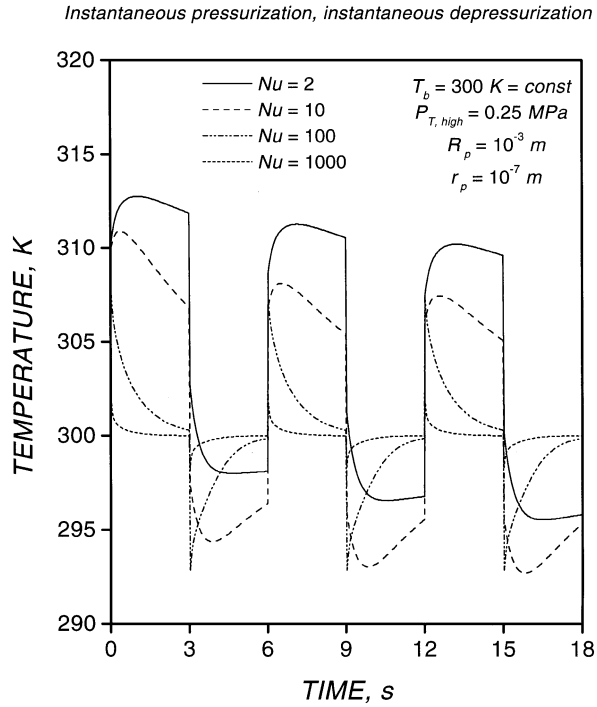

Figure 15. Temperature at the center of a sorbent particle in an infinite environment as function of time for the first three cycles with instantaneous pressurization/depressurization. Effect of the external mass transport limitations for very high heats of adsorption.

comparable to the maximum internal temperature difference, even for Nu = 2. This result may seem surprising because the effective thermal conductivity of the sorbent is by more than an order of magnitude larger than the thermal conductivity of the gas mixture, and since the heat transport in the adsorbing particles occurs primarily by conduction, for comparable length scales for heat transport in the particle and in the gas phase (i.e., Nu = 2) one would expect much higher temperature differences between the external surface of the particle and the bulk of the gas phase than between the center of the particle and the external surface of the particle. The obtained results can be explained by the fact that the heat generation or absorption in the sorbent particle is a transient effect, and as Figs. 12 and 13 show, after the fast dynamics of the adsorption or the desorption process die out, the internal temperature differences are negligible in comparison to the external ones, which is in agreement with the expectations based on the difference in the thermal conductivities.

It has been pointed out that the O_2-N_2-zeolite 5A system represents an intermediate situation with respect to the heats of adsorption (Tables 2 and 3). In order to examine the nonisothermal effects caused by higher heats of adsorption, we carried out computations in which the heats of adsorption for the O_2-N_2-zeolite 5A system were artificially increased to 50×10^6 J/kmol for both species. Heats of adsorption as high as 50×10^6 J/kmol were reported by Dunne et al. (1996) for the adsorption of CO_2 on Na-ZSM-5 and NaX zeolites. The results of these computations are presented for the conditions of Figs. 12 and 13 in Figs. 15 and 16, respectively. Qualitatively, Figs. 15 and 16 are the same as their corresponding counterparts (Figs. 12 and 13) but the maximum temperature rise (or drop) is approximately 50% higher (or lower). We observe, again, that the external and the internal maximum temperature differences are of comparable magnitude, even for Nu = 2, which points out to the conclusion that both the external and the internal temperature gradients must be accounted for when modeling the behavior of a single sorbent particle immersed in an infinite environment.

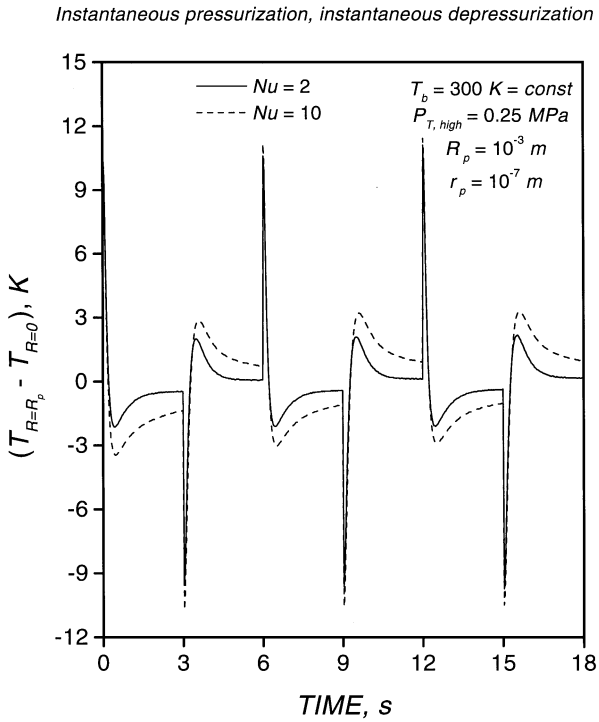

Figure 16. Temperature difference between the surface and the center of a sorbent particle in an infinite environment as function of time for the first three cycles with instantaneous pressurization/depressurization. Effect of the external mass transport limitations for very high heats of adsorption.

Results for Particles in a Finite Environment with External Heat Transport Limitations

In all the cases of a single particle in an infinite environment described so far in this study, we have assumed that what happens in the particle has no effect on the surrounding gas phase. However, this is not what happens in a packed bed where each particle interacts with a finite volume of gas phase, and therefore, the particle affects the temperature and the concentration of the adjacent gas phase. The temperature effects are stronger because not only the rate of heat transport in the bed is lower (in relative terms) than the rate of mass transport, but the thermal inertia of the particle is much larger than that of the surrounding gas phase. For bed porosity equal to 0.5, i.e., a case in which each particle interacts with an equal volume of gas phase, the overall heat capacity of the particle is larger than the overall capacity of the gas by approximately three orders of magnitude. This observation suggests that the temperature of the bulk gas phase in the bed will respond much faster then that of the particle.

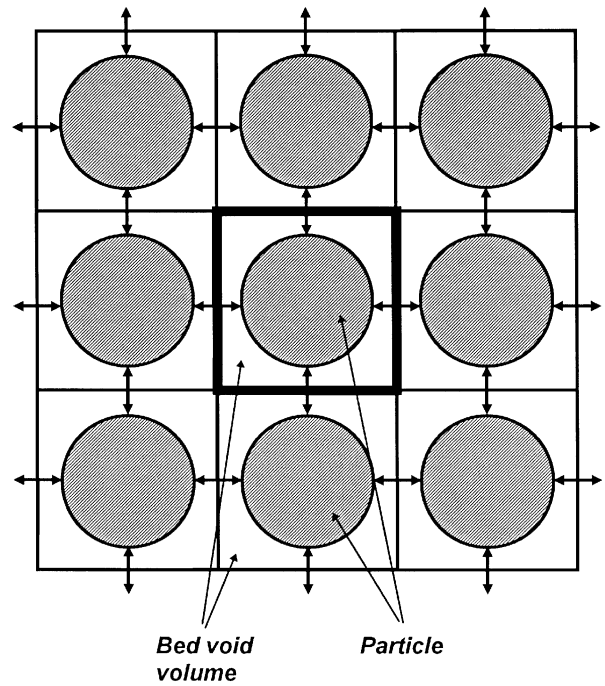

Figure 17. Two dimensional picture of the "particle-in-a-box" model.

In order to study the behavior of the sorbent particles in a packed bed using a single particle model, we propose a more realistic approach, in which the particle is considered enclosed in a box of finite volume, as shown in Fig. 17. This "particle-in-a box" model may be viewed as a unit cell in an interacting cells model of the packed bed. Each unit cell interacts with its surrounding unit cells through mass and heat exchange. Since our focus is on the heat transport effects, we ignore the mass transport interactions within the unit cell between the particle and the gas phase and assume that the mole fractions of the components in the bulk of the cell remain constant, while their partial pressures follow the total pressure pulsing sequence.

Rigorous modeling of the heat transport in the adsorbing bed (Serbezov, 1997) leads to the equation for the gas phase temperature:

$$\left(\frac{1}{R_g T_b}\sum_{i=1}^{n}\varepsilon_b C_{pg,i}\, p_{b,i}\right)\frac{\partial T_b}{\partial t} + \sum_{i=1}^{n}\underline{N}_{b,i}\cdot\left(C_{pg,i}\nabla T_b\right) - \nabla\cdot\left(\lambda_b^e \nabla T_b\right) - \frac{3}{R_p}(1-\varepsilon_b)h_f\left(T_{R=R_p} - T_b\right) = 0 \tag{27}$$

where ε_b is the void fraction in the bed and λ_b^e is the effective thermal conductivity of the bed. The terms

$\sum_{i=1}^{n} \underline{N}_{b,i} \cdot (C_{pg,i} \nabla T_b)$ and $\nabla \cdot (\lambda_b^e \nabla T_b)$ account for the energy transported in and out of the unit cell by convection and conduction, respectively. For the purpose of this analysis it will be assumed that the heat exchanged between each cell and its neighbors is very small relative to the heat exchanged between the particles and the gas phase; this is equivalent to assuming that each cell can be treated as adiabatic. Simplification of Eq. (27), or equivalently, an independent modeling of the energy conservation in the adiabatic unit cell, yield the following equation:

$$\left(\frac{1}{R_g T_b}\sum_{i=1}^{n}\varepsilon_b C_{pg,i}\, p_{b,i}\right)\frac{\partial T_b}{\partial t} - \frac{3}{R_p}(1-\varepsilon_b)h_f \times \left(T_{R=R_p} - T_b\right) = 0 \qquad (28)$$

The use of this equation together with Eq. (6) enables us to get a complete boundary condition for the temperature equation in the particle without fixing the temperature in the bulk gas phase, T_b.

Results obtained from the "particle-in-a-box" model for instantaneous pressure pulsing in the limiting case of $\mathrm{Nu} = 2$ are presented in Figs. 18 and 19. These figures show the responses of the temperatures at the center of the particle, the surface of the particle and the bulk of the gas phase for the O_2-N_2-zeolite 5A system. The results of Fig. 18 are for the actual heats of adsorption of the two gases, whereas in Fig. 19 the heats of adsorption of the species are both increased to 50×10^6 J/kmol. It is seen that when the particle is assumed to interact with a finite volume of gas, the temperature of the gas phase follows so closely the surface temperature of the particle that the two temperatures are essentially indistinguishable from each other even when the heats of adsorption are much higher than their actual values (Fig. 19). The results in Figs. 18 and 19 can be easily used to construct $(T_{R=R_p} - T_{R=0})$ vs. time curves, like those shown in Figs. 13 and 16 for the infinite environment case. This was done and it was found that the variation of the temperature differences between the surface and the center of the particle in Figs. 18 and 19 are essentially identical to those shown in Figs. 13 and 16 for the same Nusselt number ($\mathrm{Nu} = 2$)

Almost identical surface and gas phase temperatures were obtained from computations in which the heats of adsorption of O_2 and N_2 were set at a value by an order

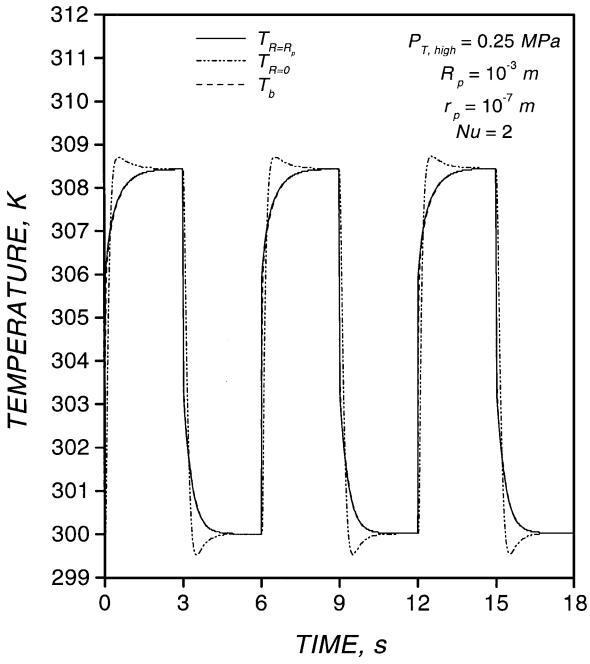

Figure 18. Temperatures at the surface, at the center, and in the bulk of the external gas phase of a sorbent particle in a finite environment with moderate heats of adsorption as function of time for the first three cycles with instantaneous pressurization/depressurization.

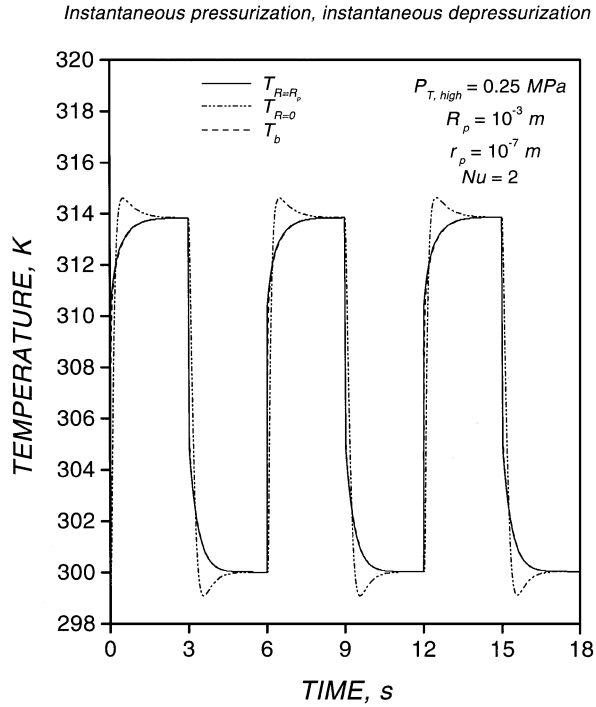

Figure 19. Temperatures at the surface, at the center, and in the bulk of the external gas phase of a sorbent particle in a finite environment with very high heats of adsorption as function of time for the first three cycles with instantaneous pressurization/depressurization.

of magnitude larger than that used in Fig. 19. The result is not surprising since, as we have already mentioned, for the typical cases that are encountered in packed beds, the heat capacity of the gas phase is by a few orders of magnitude smaller than that of the solid. Generation or absorption of heat in any adsorption process is a dynamic phenomenon, and therefore, the small thermal inertia of the gas phase enables it to track closely the temperature of the particle. These observations lead us to the conclusion that in modeling the nonisothermal operation of adsorption processes occurring in packed beds it is not necessary to allow for the temperature differences between the gas phase and the surface of the adsorbing particles. A consequence of this conclusion is that if the temperature gradients within the particles can be neglected, only a single temperature equation which is obtained from an overall local balance in the bed will be needed to describe the energy transport in the bed.

Summary and Conclusion

A general dynamic mathematical model was formulated for describing mass transport, heat transport and adsorption/desorption of multicomponent gaseous mixtures in porous particles under pressure swing conditions. A state of local equilibrium was assumed to exist between the gaseous species and the adsorbed species in the intraparticle space (i.e., macropore transport limitation only) with the adsorption isotherms being explicit in the adsorbed phase concentrations. The coupling of mass transport fluxes, temperature, partial pressures, and partial pressure gradients in the intraparticle space was described using the 3-parameter dusty-gas model. An energy equation in which both conductive and convective modes of heat transport were considered was used to describe the temperature variations within the particle.

The main focus of this study was on the nonisothermal effects in porous sorbents under pressure swing conditions. Computations were carried out for the industrially important air-zeolite 5A system. The intraparticle temperature profiles were found to increase or decrease smoothly from the surface to the center of the particle. The largest temperature differences in the particle were observed for the case of instantaneous pressure change which, however, was not a realistic pressure pulsing scheme from practical point of view. For the more realistic cases (e.g., linear pressurization/exponential depressurization and sinusoidal pressure change), the observed temperature differences in the particle were considerably smaller. These differences increased with the increase of the difference between the high and the low limit of operating pressure and with the increase of the rates for pressurization and depressurization. The intraparticle temperature differences decreased with the decrease in the particle pore size.

Two types of boundary conditions for the temperature at the outer surface of the particle were considered: a case in which the particle was immersed in an infinite environment with constant temperature, and another (particle-in-a-box model), in which the surrounding gas phase was of finite volume, and its temperature was determined by the rate at which it exchanged heat with the particle. The case of infinite environment typically arises in single particle experiments for determining the transport properties of the porous adsorbents. We have found out that in this case the external and the internal temperature gradients are equally important, and therefore, both must be accounted for in the mathematical models used to extract the transport data from the experimental results.

The particle-in-a-box model was representative for the situation in packed bed adsorption columns. For this case we found out that the temperatures in the bulk of the bed and at the outer surface of the particles were essentially identical for a wide range of heats of adsorption. We concluded that in the modeling the nonisothermal operation of adsorption processes occurring in packed beds it was not necessary to allow for the temperature differences between the gas phase and the surface of the adsorbing particles. Furthermore, if the temperature gradients within the particles can be neglected, only a single temperature equation which is obtained from an overall local balance in the bed will be needed to describe the energy transport in the bed.

Notation

a_i	Constant in the adsorption isotherm defined in Eq. (9)	—
B^e	Effective permeability of the adsorbing particle	m^2
$\mathbf{B}$	Matrix defined in Eqs. (15) and (16)	—
$C_{pg,i}$	Specific heat capacity of species i in the gas phase	J/kmol·K
$C_{pq,i}$	Specific heat capacity of species i in the adsorbed phase	J/kmol·K
C_{ps}	Specific heat capacity of the solid material	J/kg·K

d_i	Constant in the adsorption isotherm defined in Eq. (9)	K
D^e	Effective mass transport coefficient in Eqs. (24) and (25)	m^2/s
$D_{K,i}$	Knudsen transport coefficient of species i	m^2/s
$\mathscr{D}_{i,j}$	Binary diffusion coefficient for gases i and j	m^2/s
F	Matrix defined in Eqs. (17) and (18)	—
h_f	Heat transfer coefficient	$J/m^2{\cdot}s{\cdot}K$
h_i	Adsorption equilibrium coefficient in Eq. (9)	—
$k_{g,\mathrm{mix}}$	The thermal conductivity of the gas mixture	J/m·s·K
$(-\Delta H_i)$	Equilibrium heat of adsorption of species i	J/kmol
M	Molecular mass (used in Table 1)	—
n	Number of species in the gaseous mixture	—
$\underline{N}_i$	Molar flux of species i relative to stationary coordinates	$kmol/m^2{\cdot}s$
$\underline{\mathbf{N}}$	Vector of $\underline{N}_i$	$kmol/m^2{\cdot}s$
Nu	Nusselt number defined in Eq. (26)	—
P_T	Total pressure	Pa
p_i	Partial pressure of species i	Pa
p	Vector of the partial pressures	Pa
q_i	Solid phase concentration of species i	$kmol/m^3$
r_p	Particle pore size	m
R_g	Ideal gas law constant	J/kmol·K
R_p	Radius of the adsorbing particles	m
$t_{1/2}$	Half cycle time	s
T	Temperature	K
y_i	Mole fraction of species i	—

Greek Letters

γ	Parameter in Eq. (24),	s^{-1}
ε_b	Porosity of the adsorbing bed	—
ε_p	Porosity of the adsorbing particles	—
η	Tortuosity factor	—
λ^e	Effective thermal conductivity of the sorbent particle	J/m·s·K
λ_b^e	Effective thermal conductivity of the adsorbing bed	J/m·s·K
μ	Viscosity of the gaseous mixture	kg/m·s
ρs	Density of the solid material	kg/m^3

Subscript

b	Quantities referring to the bulk gas phase or to the bed

Superscripts

e	Effective quantities
$\hat{}$	Reference quantities

References

Alpay, E., C.N. Kenney, and D.M. Scott, "Simulation of a Rapid Pressure Swing Adsorption and Reaction Processes," *Chem. Engng. Sci.*, **48**, 3173–3186 (1993).

Brunovska, A., V. Hlavacek, J. Ilavsky, and J. Valtyni, "An Analysis of a Nonisothermal One-Component Sorption in a Single Adsorbent Particle," *Chem. Engng. Sci.*, **33**, 1385–1391 (1978).

Chihara, K., M. Suzuki, and K. Kawazoe, "Effect of Heat Generation on Measurement of Adsorption Rate by Gravimetric Method," *Chem. Engng. Sci.*, **31**, 505–507 (1976).

De Boor, C.A., *A Practical Guide to Splines*, Springer-Verlag, New York, 1978.

Dunne, J.A., R. Mariwala, M. Rao, S. Sircar, R.J. Gorte, and A.L. Myers, "Calorimetric Heats of Adsorption and Adsorption Isotherms. 1. O_2, N_2, Ar, CO_2, CH_4, C_2H_6, and SF_6 on NaX, H-ZSM-5, and Na-ZSM-5 Zeolites," *Langmuir*, **12**, 5896–5904 (1996).

Farooq, S., M.N. Rathor, and K. Hidajat, "A Predictive Model for a Kinetically Controlled Pressure Swing Adsorption Separation Process," *Chem. Engng. Sci.*, **48**, 4129–4141 (1993).

Gear, C.W., *Numerical Initial Value Problems in Ordinary Differential Equations*, Prentice Hall, Englewood Cliffs, NJ, 1971.

Haq, N. and D.M. Ruthven, "A Chromatographic Study of Sorption and Diffusion in 5A Zeolite," *J. Colloid Interface Sci.*, **112**, 164–169 (1986).

Haul, R. and H. Stremming, "Nonisothermal Sorption Kinetics in Porous Adsorbents," *J. Colloid Interface Sci.*, **97**, 348–355 (1984).

Hu, X. and D.D. Do, "Validity of Isothermality in Adsorption Kinetics of Gases in Bidispersed Solids," *A.I.Ch.E. J.*, **41**, 1581–1584 (1995).

Ilavsky, J., A. Brunovska, and V. Hlavacek, "Experimental Observation of Temperature Gradients Occurring in a Single Zeolite Pellet," *Chem. Engng. Sci.*, **35**, 2475–2479 (1980).

Jackson, R., *Transport in Porous Catalysts*, Elsevier, New York, 1977.

Kondis, E.F. and J.S. Dranoff, "Nonisothermal Sorption of Ethane by 4A Molecular Sieves," *AIChE Symp. Ser.*, **67**(117), 25–34 (1971).

Lee, K.-L. and D.M. Ruthven, "Analysis of Thermal Effects in Adsorption Rate Measurements," *J. Chem. Soc. Faraday I*, **75**, 2407–2422 (1979).

Lopes, J.C., M.M. Dias, V.G. Mata, and A.E. Rodrigues, "Flow Field and Non-Isothermal Effects on Diffusion, Convection, and Reaction in Permeable Catalysts," *Ind. Engng. Chem. Res.*, **34,** 148–157 (1995).

Mason, E.A. and A.P. Malinauskas, *Gas Transport in Porous Media: The Dusty-Gas Model*, Elsevier, New York, 1983.

Miller, G.W., K.S. Knaebel, and K.G. Ikels, "Equilibria of Nitrogen, Oxygen, Argon, and Air in Molecular Sieve 5A," *A.I.Ch.E. J.*, **33**, 194–201 (1987).

Ofori, J.Y. and S.V. Sotirchos, "Dynamic Convection-Driven Thermal Gradient Chemical Vapor Infiltration," *J. Mater. Res.*, **11**, 2541–2555 (1996).

Ruthven, D.M., L.-K. Lee, and H. Yucel, "Kinetics of Non-Isothermal Sorption in Molecular Sieve Crystals," *A.I.Ch.E. J.*, **26**, 16–23 (1980).

Ruthven, D.M. and Z. Xu,"Diffusion of Oxygen and Nitrogen in 5A Zeolite Crystals and Commercial 5A Pellets," *Chem. Engng. Sci.*, **48**, 3307–3312 (1993).

Serbezov, A., Ph.D. Dissertation, University of Rochester, Rochester, NY, 1997.

Serbezov, A.S. and S.V. Sotirchos, "Multicomponent Pressure Swing Adsorption: Semianalytical Solution for Local Equilibrium and Comparison with the Predictions of a Generalized Multicomponent Model," *A.I.Ch.E. Meeting*, San Francisco, 1994.

Serbezov, A. and S.V. Sotirchos," Multicomponent Transport Effects in Sorbent Particles under Pressure Swing Conditions," *Ind. Engng. Chem. Res.*, **36**, 3002–3012 (1997a).

Serbezov, A. and S.V. Sotirchos, "Generalized Linear Driving Force Approximation for Modeling Multicomponent Adsorption-Based Separations," Submitted for publication (1997b).

Sorial, G.A., W.H. Granville, and W.O. Daly, "Adsorption Equilibria for Oxygen and Nitrogen Gas Mixtures on 5A Molecular Sieves," *Chem. Engng. Sci.*, **38**, 1517–1523 (1983).

Sotirchos, S.V., "Multicomponent Diffusion and Convection in Capillary Structures," *A.I.Ch.E. J.*, **35**, 1953–1961 (1989).

Sotirchos, S.V., "Dynamic Modeling of Chemical Vapor Infiltration," *A.I.Ch.E. J.*, **38**, 1365–1378 (1991).

Sotirchos, S.V. and N.R. Amundson, "Dynamic Behavior of a Porous Char Particle Burning in an Oxygen-Containing Environment," *A.I.Ch.E. J.*, **30**, 537–548 (1984a).

Sotirchos, S.V. and N.R. Amundson, "Part II: Transient Analysis of a Shrinking Particle," *A.I.Ch.E. J.*, **30**, 549–556 (1984b).

Sun, L.M. and F.A. Meunier, "Detailed Model for Nonisothermal Sorption in Porous Adsorbents," *Chem. Engng. Sci.*, **42**, 1585–1593 (1987).

Tomadakis, M.M. and S.V. Sotirchos, "Ordinary, Transition, and Knudsen Regime Diffusion in Random Capillary Structures," *Chem. Engng. Sci.*, **48**, 3323–3333 (1993).